SOCIAL MEMORY

Ventral CA1 neurons store social memory

Teruhiro Okuyama,[1] Takashi Kitamura,[1] Dheeraj S. Roy,[1] Shigeyoshi Itohara,[2] Susumu Tonegawa[1,2,3]*

The medial temporal lobe, including the hippocampus, has been implicated in social memory. However, it remains unknown which parts of these brain regions and their circuits hold social memory. Here, we show that ventral hippocampal CA1 (vCA1) neurons of a mouse and their projections to nucleus accumbens (NAc) shell play a necessary and sufficient role in social memory. Both the proportion of activated vCA1 cells and the strength and stability of the responding cells are greater in response to a familiar mouse than to a previously unencountered mouse. Optogenetic reactivation of vCA1 neurons that respond to the familiar mouse enabled memory retrieval and the association of these neurons with unconditioned stimuli. Thus, vCA1 neurons and their NAc shell projections are a component of the storage site of social memory.

The ability to recognize and memorize familiar conspecifics (social memory) is crucial for animals that exhibit social interactions (*1*, *2*). Lesion and recording studies in humans and monkeys have suggested that the medial temporal lobe or the hippocampus plays an essential role in social memory (*3*–*6*). In mice, most early lesion or recording studies concluded that the hippocampus is dispensable for recognizing a familiar conspecific (*7*–*9*), whereas a few recent studies suggested the contrary (*10*–*12*). Although these human and animal studies identified brain areas important for social memory, the precise cellular populations storing this type of memory and their essential circuits are unknown.

The intrinsic pattern of connectivity in the hippocampus is fairly invariable along the longitudinal axis (*13*) across many species (*14*). However, the afferent and efferent connectivity along this axis changes from one end to the other, suggesting that dorsal and ventral hippocampus of rodents (corresponding to posterior and anterior hippocampus, respectively, of primates) may have distinct functions (*14*, *15*). It is well established that the rodent dorsal hippocampus (dHPC) plays an essential role in episodic memory (*15*). In contrast, the memory function of the ventral hippocampus (vHPC) is poorly known. In this study, we generated a transgenic mouse line, transient receptor potential channel 4–Cre (Trpc4-Cre), to investigate the potential role and physiological characteristics of the pyramidal neurons in the CA1 subfield of the ventral hippocampus (vCA1) in social memory.

Mice naturally spend more time interacting with a previously unencountered ("novel") mouse than a familiar one (*16*); social memory can be quantified by measuring the relative interaction durations with a novel and a familiar mouse under free-choice conditions (social discrimination test or SDT) (Fig. 1, A and B). This ability to socially discriminate between the novel and familiar mice persisted for 30 min after a familiarization session, but disappeared by 24 hours (Fig. 1C). To investigate the potential role of vHPC and dHPC in social memory, we targeted bilateral injections of adeno-associated virus 8 (AAV8)–calcium/calmodulin-dependent protein kinase II (CaMKII):eArchT–enhanced yellow fluorescent protein (EYFP) and optic fiber implants to vCA1 or dorsal CA1 (dCA1) of wild-type mice (Fig. 1D). Expression of eArchT-EYFP was abundant in vCA1 or dCA1, although it was also observed to a lesser extent in CA3 and the dentate gyrus (DG) (Fig. 1, E and F). Optogenetic cell body inhibition of vHPC but not dHPC resulted in a deficit in the SDT (Fig. 1, G, H, O, and P). In the resident-intruder test (Fig. 1I and fig. S1), optogenetic inhibition of vHPC but not dHPC increased the sniffing duration toward a familiar intruder with no effect when a novel intruder was used (Fig. 1, J and K).

To identify downstream brain region(s) involved in social memory, we injected AAV9–tetracycline response element (TRE):channelrhodopsin-2 (ChR2)–EYFP into vCA1 of c-fos:tetracycline transactivator (tTA) mice to label neurons activated by social interaction (*17*, *18*). NAc shell, olfactory bulb (OB), and basolateral amygdala (BLA) were the major targets of the social interaction–specific vCA1 neuronal projections (fig. S2). Moreover, retrograde tracer cholera toxin subunit B (CTB)–Alexa555 injection into NAc, OB, or BLA labeled vCA1 but not dCA1 neurons (fig. S3). We then examined whether any of these projections are necessary for social memory by bilaterally injecting AAV8-CaMKII:eArchT-EYFP into vHPC and then optogenetically inhibiting axonal terminals of the vCA1 neurons in the respective target areas while the mice went through the SDT (Fig. 1, L to N, Q to S, and fig. S4). vHPC-NAc projections, but not vHPC-OB or vHPC-BLA, were essential for social discrimination behavior.

To more rigorously establish the functional role of the vCA1-NAc connection, we generated a CA1 pyramidal cell–specific Cre mouse line, Trpc4-Cre, that covers both vCA1 and dCA1 (fig. S5 and Methods). Using Trpc4-Cre mice, we selectively targeted vCA1 excitatory pyramidal neurons by injecting AAV9–human synapsin (hsyn): double-floxed inverse open reading frame (DIO)–eArchT-EYFP into vCA1 (Fig. 2, A and B, and fig. S6). We confirmed that the vCA1 neurons specifically project to the NAc shell but not to the NAc core, as identified by tyrosine hydroxylase (TH) staining (Fig. 2C). Further, CTB injection into NAc labeled the Trpc4-expressing deep layer (vCA1d), but not the superficial layer (vCA1s), pyramidal cells in vCA1 (Fig. 2B). Bilateral injections of AAV9-hsyn:DIO-eArchT-EYFP into the vCA1 of Trpc4-Cre mice and optogenetic inhibition of vCA1 cell body (Fig. 2, D and H) or its axonal terminals in NAc (Fig. 2, F, G, and J) resulted in a SDT deficit similar to that observed by vHPC-NAc inhibition (compare Fig. 2G with Fig. 1L). Optogenetic inhibition of vCA1 cell body during the familiarization period also led to a similar SDT defect (fig. S8). The possibility that these deficits are due to inhibition of dorsal CA2 (dCA2) activity is excluded because dCA2 is unlabeled with eArchT-EYFP in these mice (fig. S6C). dCA1 cell body inhibition was carried out using Wfs1-Cre mouse line expressing Cre in dCA1 but not in vCA1 or dCA2 (fig. S9) (*19*), which showed no deficit in a SDT (Fig. 2, E and I).

Inhibition of vCA1-NAc shell projections in Trpc4-Cre mice only during the interaction with a novel mouse did not affect the SDT (Fig. 2K, middle, and fig. S7A), whereas inhibition only during interaction with a familiar mouse disrupted social discrimination between the two mice (Fig. 2K, right, and fig. S7A). In contrast, when a pair of novel mice (Fig. 2L and fig. S7B), novel and familiar objects (fig. S10A), or novel and familiar contexts (fig. S10B) were used, there was no effect of vCA1-NAc shell inhibition.

We performed a SDT using Trpc4-Cre mice expressing AAV9–elongation factor 1α (EF1α):DIO-ChR2-EYFP in vCA1 while stimulating vCA1-NAc shell projections (Fig. 2, M and N, and fig. S7). Optogenetic activation of vCA1-NAc shell terminals during social interaction with a novel mouse disrupted the SDT (Fig. 2M, middle, and fig. S7C). With a pair of novel mice as the targets, stimulating vCA1-NAc shell projections during interactions with one of the novel mice greatly reduced the sniffing duration of that mouse compared to the other novel mouse (Fig. 2N and fig. S7D). Optogenetic activation of vCA1-NAc shell terminal during interaction with a familiar mouse had no effect in the SDT (Fig. 2M, right, and fig. S7C). Light activation did not affect the SDT in the EYFP control groups (fig. S11, A and B). With novel objects in place of mice, interactions of the test mouse were not affected by activation of the vCA1-NAc shell projections (fig. S11C).

[1]RIKEN–MIT Center for Neural Circuit Genetics at the Picower Institute for Learning and Memory, Department of Biology and Department of Brain and Cognitive Sciences, Massachusetts Institute of Technology (MIT), Cambridge, MA 02139, USA. [2]Brain Science Institute, RIKEN, Saitama, 351-0198, Japan. [3]Howard Hughes Medical Institute at MIT, Cambridge, MA 02139, USA.
*Corresponding author. Email: tonegawa@mit.edu

These results suggest that increased activation of the vCA1-NAc shell projections while the test mouse was in the novel-mouse domain disrupted the discriminatory social behavior by making the test mouse perceive the novel mouse as familiar.

To monitor the activity of vCA1 cells before and after the familiarization of a conspecific mouse, we injected AAV5-hsyn:DIO-GCaMP6f into the vCA1 of Trpc4-Cre mice and implanted a microprism grin lens targeting the pyramidal cell layer in vCA1 (Fig. 3, A and B; see Methods) (*20*, *21*). Ca^{2+} events in vCA1 neurons (Fig. 3, D and E) were recorded during exposure to two novel mice (A and B) in two consecutive 5-min sessions with mouse A and mouse B in counterbalanced positions, followed by a 5-min control session with no mice (Before group). The test mice were subjected to 3-day-long or 2-hour-long familiarization with mouse A, and the recording sequence was repeated after 30 min or 24 hours' separation (After-1 group) (Fig. 3F). For each neuron, we calculated a "preference score" based on the head position of the test mouse during each recorded Ca^{2+} event and identified vCA1 cells that exhibited selective activation by mouse A or mouse B (Fig. 3G and fig. S12). There was a significant increase in the proportion of mouse-A neurons after 3 days' or 2 hours' familiarization to mouse A (Fig. 3H). In contrast, there was no effect of familiarization on the proportion of cells active around mouse sampling locations in control sessions (No mouse). Similarly, familiarization had no effect on the proportion of mouse-A neurons in dCA1 of Wfs1-Cre transgenic mice (Fig. 3, C and H).

We determined the preference score of mouse-A neurons in Before group and After-1 group, as well as After-2 group that had a second 3-day familiarization. The preference scores of individual mouse-A neurons were not correlated between Before group and After-1 group, whereas these scores were correlated between After-1 group and After-2 group (Fig. 3, I to L). In addition, mouse-A neurons of After-1 group showed an increase in Ca^{2+} event probability around the mouse-A sniffing area, whereas mouse-A neurons did not show such an increase in Ca^{2+} probability in the mouse B sniffing area (Fig. 3M). Although the individual mouse-A neurons were still significantly activated by mouse A (Fig. 3, N

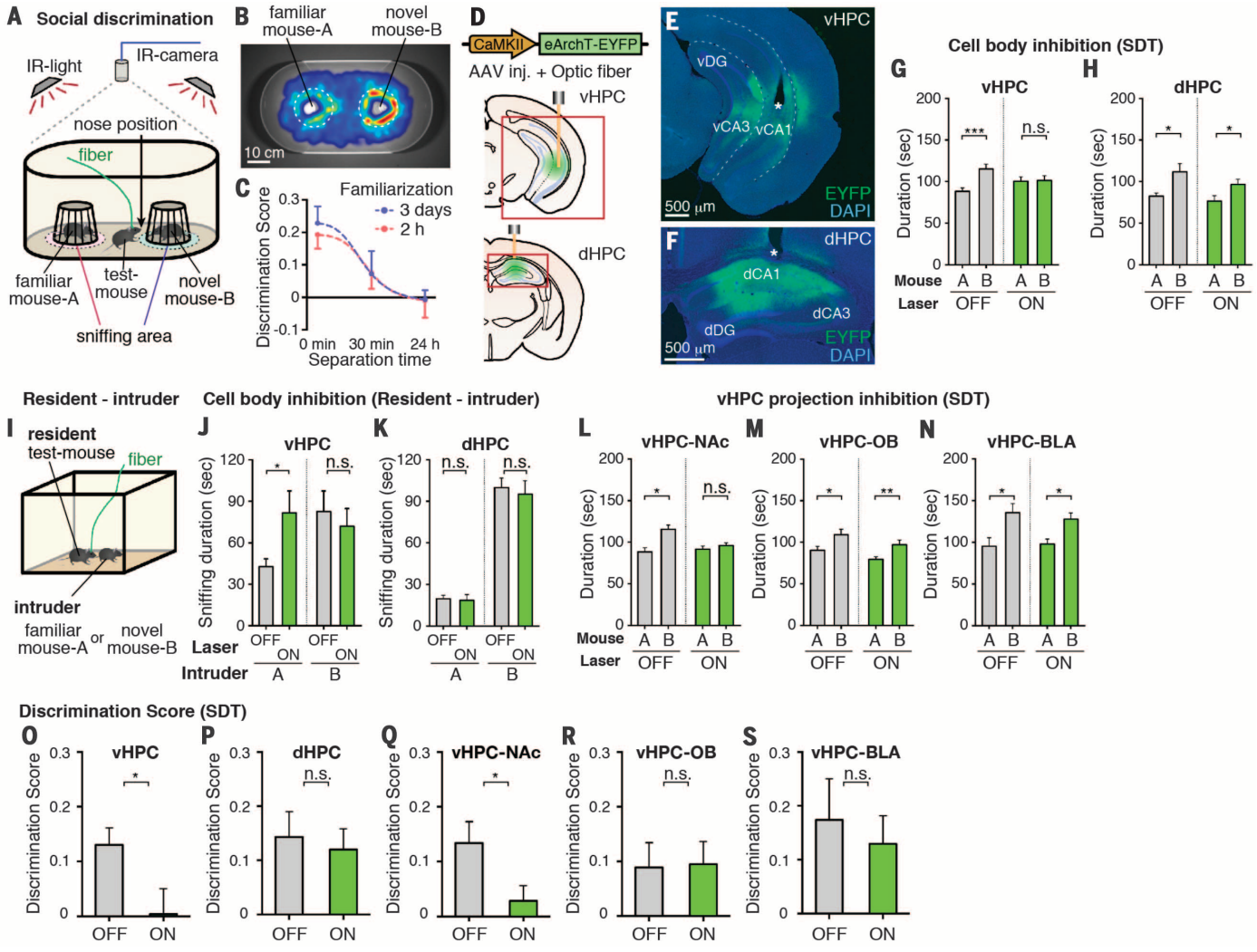

Fig. 1. vHPC in social memory. (**A**) Social discrimination test (SDT). (**B**) Representative heat map of test-mouse position during the SDT. (**C**) Kinetics of the SDT (see Methods). (**D** to **F**) Expression of AAV8-CaMKII:eArchT-EYFP (green) in vHPC or dHPC of wild-type mice. Asterisk indicates optic fiber tip. (**G** and **H**) Total duration in the sniffing area of familiar mouse A or novel mouse B during a SDT with inhibition of vHPC [(G) and (O), $n = 17$ mice] or dHPC [(H) and (P), $n = 14$ mice]. (**I**) Resident-intruder test. (**J** and **K**) Total sniffing duration by the resident to intruder [(J), vHPC inhibition; (K), dHPC inhibition] in familiar-intruder group (left) and novel-intruder group (right) ($n = 7$ mice, each group). (**L** to **N**) Total duration in sniffing area during a SDT observed in wild-type mice bilaterally injected with AAV8-CaMKII:eArchT-EYFP into vHPC and implanted with optical fibers targeting NAc [(L) and (Q), $n = 23$ mice], OB [(M) and (R), $n = 16$ mice], or BLA [(N) and (S), $n = 13$ mice]. (**O** to **S**) Comparison of discrimination scores. Green bars, laser on; gray bars, laser off. Significance for multiple comparisons: paired t test, $^{*}P < 0.05$; $^{**}P < 0.01$; $^{***}P < 0.001$, n.s., not significant. Data presented as mean ± SEM.

and O), Ca^{2+} event probability of these neurons in mouse-A area was reduced when the recordings were conducted after 24 hours' separation following familiarization (Fig. 3P).

The c-fos:tTA/TRE system permits labeling and manipulations of memory engram cells (*17*, *22*). We used this technology to characterize mouse-A neurons. First, we injected AAV9-TRE:fluorescent timer (FT)–Slow into the vCA1 of c-fos:tTA mice and induced expression of FT-Slow in neurons activated by social interaction (Fig. 4A). The fluorescence of FT-Slow changes naturally over time (*23*), from blue (pseudo-green), 12 hours after induction, to red, 72 hours after induction (Fig. 4, A and B, and fig. S13). Test mice interacted with mouse A twice, or with mouse A and then mouse B, with a 72-hour separation (Fig. 4, C and D). The proportions of reactivated cells with an overlap of red and blue signal was significantly higher in test mice exposed to the same mouse A twice, versus those exposed to mouse A followed by mouse B (Fig. 4E and fig. S13). A similar quantitative analysis of vCA1 reactivation using H2B-EGFP [nuclear localized EGFP (enhanced green fluorescent protein)] and c-Fos expression showed comparable results (fig. S14).

Second, we targeted injection of AAV9-TRE:ChR2-EYFP and optic fibers to vCA1 of c-fos:tTA mice and labeled vCA1 cells that were activated by 2 hours of exposure to a mouse A with ChR2 while the c-fos:tTA mouse was off doxycycline (OFF-Dox) (Fig. 4, F and G, and fig. S2). As expected, social memory was absent in the SDT conducted after 24 hours' separation (Fig. 4H, left), but was present when blue light was shone to the whole test box (Fig. 4H, right). Control experiments conducted with no ChR2 mice (Fig. 4I) or a pair of novel mice during the SDT (fig. S15A) did not show social memory. Restricting blue light to mouse-A area but not mouse-B area also caused the restoration of social memory (Fig. 4J). These results suggest that even after social memory cannot be retrieved by natural cues, the memory engram cells for the familiar mouse are sufficiently retained and can be reactivated optogenetically for memory retrieval (*17*, *24*). Indeed, the proportion of mouse-A neurons reactivated by blue light is much greater than that reactivated by natural cues (i.e., mouse A) after a 3-day separation (compare fig. S16G and Fig. 4E). We further investigated the parameters that affect social memory, including the postfamiliarization separation periods, the proportion of reactivated familiar mouse-A neurons, the nature of recall cues (natural versus optogenetic), and the strength of the reactivation methods (figs. S14 and S16). The data indicate that optogenetic stimulation is more effective than natural stimulation in reactivating memory engram cells and that a certain minimum threshold level of reactivation of mouse-A neurons will have to be reached for social memory to be expressed in the SDT paradigm.

Third, we used the memory inception protocol (Fig. 4K) (*22*). After 24 hours' separation, ChR2-labeled mouse-A neurons were light-activated simultaneously with foot-shock delivery [i.e., negative unconditioned stimulus (US)] or cocaine administration (i.e., positive US). The test mouse exhibited avoidance or approach behavior toward mouse A, respectively, in a SDT conducted the next day (Fig. 4, K to N). Negative control groups with no ChR2 (i.e., AAV9-TRE:EYFP alone) (Fig. 4, O and P) or no US (fig. S15B) did not show any behavioral alterations. No avoidance or approaching behavior was observed when two novel mice (B and B') were used as the target mice during the test (fig. S15, C and D). AAV9-TRE:ChR2-EYFP injection into dCA1 of c-fos:tTA mice did not lead to memory inception (fig. S17).

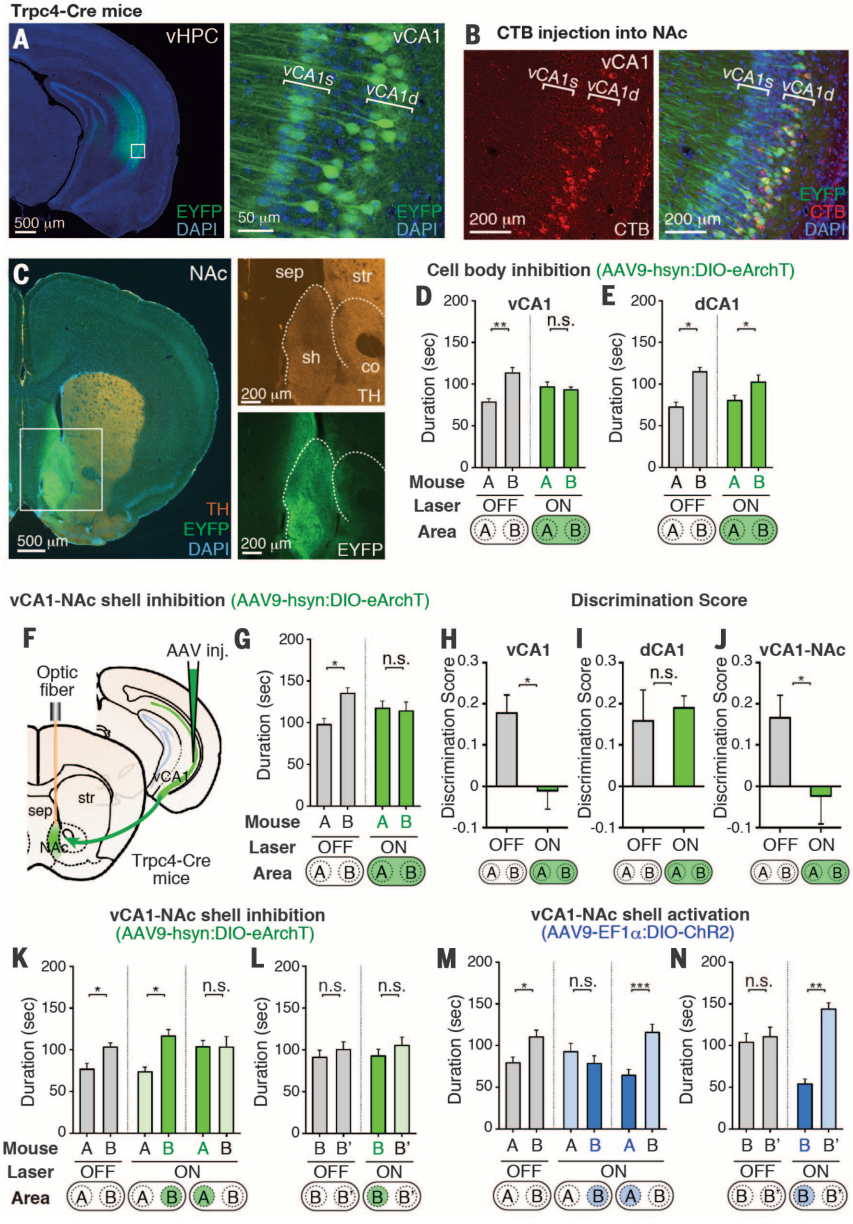

Fig. 2. vCA1-NAc circuit in a SDT. (**A**) Coronal vHPC sections of a Trpc4-Cre mouse injected with AAV9-hsyn:DIO-eArchT-EYFP into vCA1, stained with anti-GFP (green) and DAPI (4′,6-diamidino-2-phenylindole, blue). (**B**) CTB-Alexa555 (red) injection into NAc and stained with anti-GFP (green) and DAPI (blue). (**C**) Coronal NAc sections of a Trpc4-Cre mouse injected with AAV9-hsyn:DIO-eArchT-EYFP into vCA1, stained with anti-GFP (green), anti-TH (orange), and DAPI (blue). NAc shell (sh); NAc core (co); septum (sep); striatum (str). Boxed areas in (A) and (C) are magnified. (**D** and **E**) Cell body inhibition of vCA1 and dCA1 during a SDT in Trpc4-Cre and Wfs1-Cre mice, respectively. (**F**) Manipulation of vCA1-NAc shell projections. (**G** and **K** to **N**) SDT in Trpc4-Cre mice during vCA1-NAc manipulation. vCA1 injections of AAV9-hsyn:DIO-eArchT-EYFP [(G), n =14 mice; (K) and (L), each n = 12 mice] and AAV9-EF1α:DIO-ChR2-EYFP [(M) and (N), each n = 14 mice]. (**H** to **J**) Comparison of discrimination scores. Bottom, targeting area for the laser stimulation. Mouse A, familiar mouse; mouse B and -B', novel mouse. Green bars, green laser on; blue bars, blue laser on; gray bars, laser off. Significance for multiple comparisons: paired t test, $^*P < 0.05$; $^{**}P < 0.01$; n.s., not significant. Data presented as mean ± SEM.

The possibility that the observed optogenetic recall or memory inception is due to memory held in adjacent dCA2 is excluded because no labeling of dCA2 cells with ChR2 could be observed under our experimental conditions (fig. S17, D to F).

We have established that vCA1 and its projections to NAc shell play a necessary and sufficient role in social memory in the mouse. Furthermore, we have provided evidence that vCA1 pyramidal cells hold the memory of a familiar mouse; a population of vCA1 pyramidal cells are activated by exposure to a familiar mouse, a large fraction of these cells are reactivated by reexposure to the same mouse, and optogenetic reactivation of the vCA1 cells previously activated by exposure to a familiar mouse elicited recall of the specific social memory as

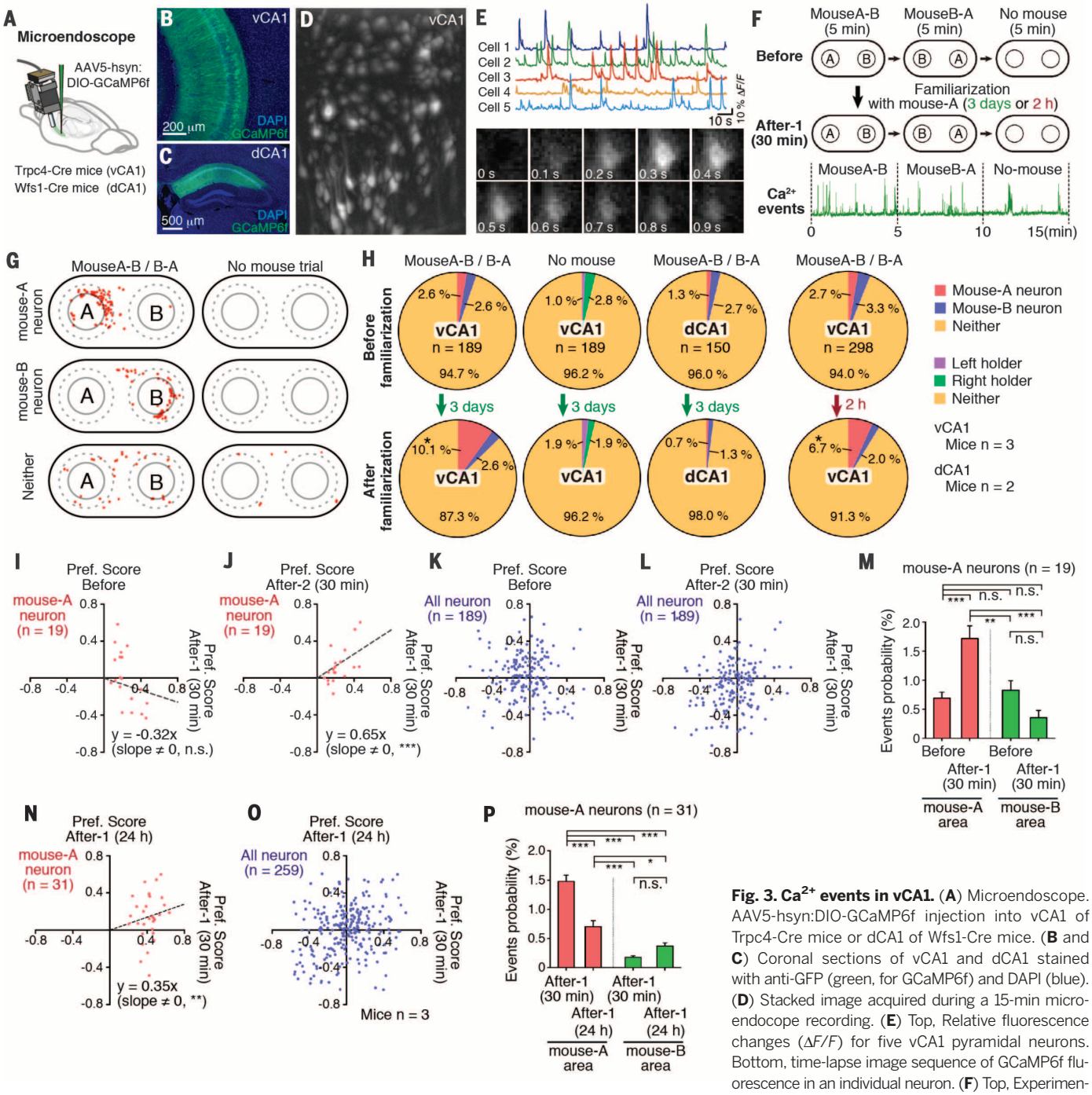

Fig. 3. Ca^{2+} events in vCA1. (**A**) Microendoscope. AAV5-hsyn:DIO-GCaMP6f injection into vCA1 of Trpc4-Cre mice or dCA1 of Wfs1-Cre mice. (**B** and **C**) Coronal sections of vCA1 and dCA1 stained with anti-GFP (green, for GCaMP6f) and DAPI (blue). (**D**) Stacked image acquired during a 15-min microendocope recording. (**E**) Top, Relative fluorescence changes ($\Delta F/F$) for five vCA1 pyramidal neurons. Bottom, time-lapse image sequence of GCaMP6f fluorescence in an individual neuron. (**F**) Top, Experimental protocol for microendoscope recording. Bottom, relative fluorescence changes during 15-min recording. (**G**) Representative mouse-A neuron, mouse-B neuron, and neither neuron. Head position at each Ca^{2+} event (red dots). (**H**) Proportion of mouse-A, mouse-B, or neither neurons in vCA1 and dCA1, before and after familiarization (3 days or 2 hours) (chi-square test, $^{*}P < 0.05$). (**I** to **L** and **N** to **O**) Comparison of the preference scores of mouse-A neurons [(I), (J), and (N), red dots) and all recorded neurons [(K), (L), and (O), blue dots] between After-1 (30 min) and Before sessions [(I) and (K); linear regression, $P = 0.208$], between After-1 (30 min) and After-2 (30 min) [(J) and (L), linear regression, $P = 0.0002$; Spearman rank correlation test, $r = 0.65$), and between After-1 (30 min) and After-1 (24 hours) [(N) and (O), linear regression, $P = 0.0019$; Spearman rank correlation test, $r = 0.23$). (**M** and **P**) Comparison of Ca^{2+} event probabilities of mouse-A neurons [analysis of variance (ANOVA); post-hoc, Scheffe, $^{***}P < 0.001$, $^{**}P < 0.01$). Data presented as mean ± SEM.

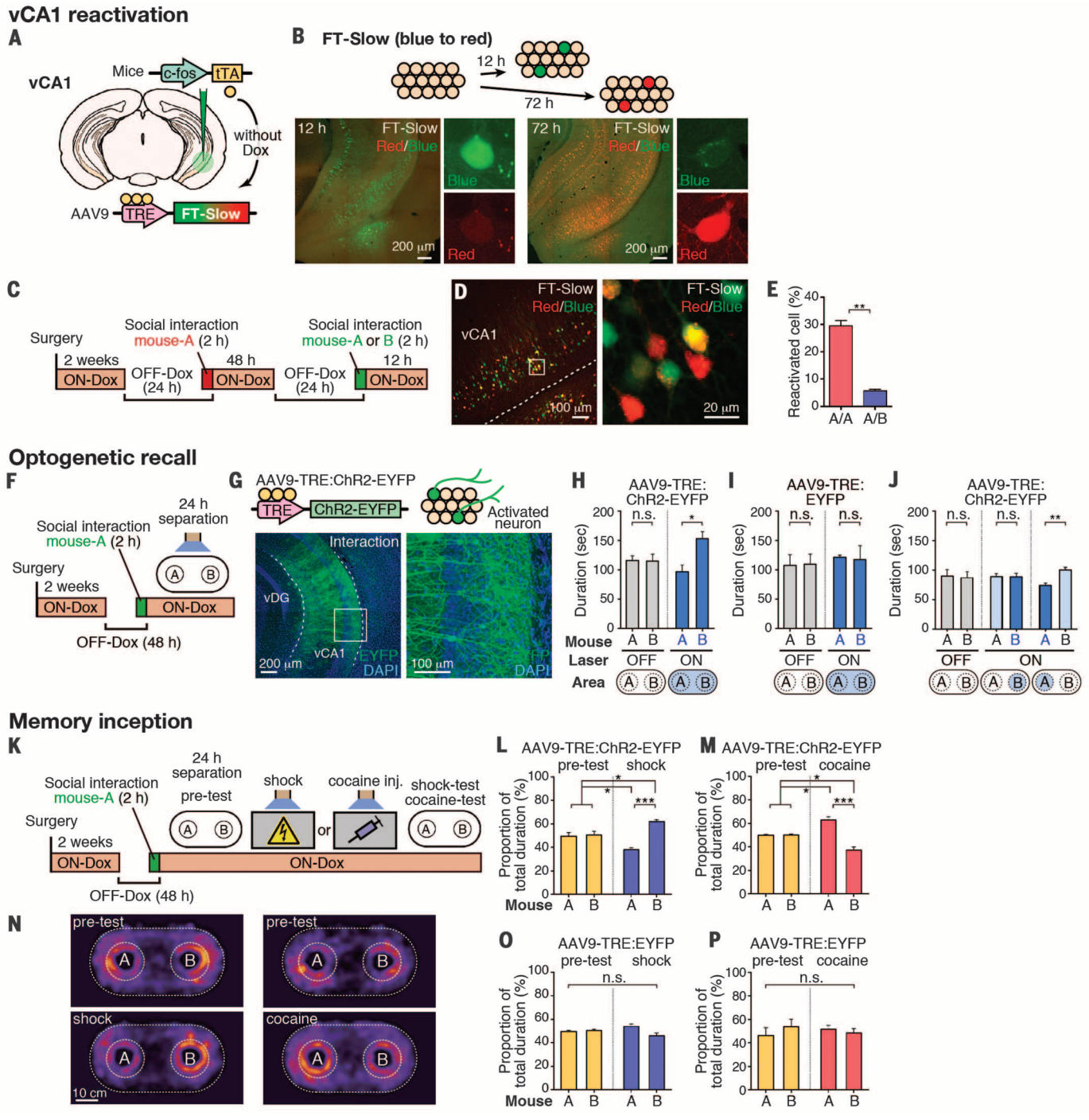

Fig. 4. Social-memory engrams. (**A**) Activity-dependent labeling method. (**B**) Injection of AAV9-TRE:FT-Slow into vCA1 of c-fos:tTA mice. Top, fluorescent color alteration of FT-Slow. Bottom, coronal vCA1 sections 12 hours (left) and 72 hours (right) after induction. Representative images of a blue-form (pseudo-green color)– or red-form (red)–expressing cell. (**C**) Protocol for visualizing two activated neuronal populations. (**D**) FT-Slow blue form–, red form–, and double (yellow)–positive cells in vCA1 (left) with magnified image (right). (**E**) Percentage of reactivated cells when the test mouse was exposed to the same mouse A twice (A/A) or mouse A and then mouse B (A/B) (n = 3 mice, each group). (**F**) Protocol for optogenetic recall of social-memory engram. (**G**) vCA1 section of c-fos:tTA mice injected with AAV9-TRE:ChR2-EYFP showing ChR2-labeling by social interaction. (**H** to **J**) SDT with or without activation of engram cells. Blue bars, blue laser on; gray bars, laser off. Bottom, targeting area for the laser stimulation. (**K**) Protocol for memory inception. (**L**, **M**, **O**, and **P**) Proportion of total duration in the sniffing area of mouse A or mouse B (yellow bars, pretest; blue bars, shock test; red bars, cocaine test). c-fos:tTA mice injected with AAV9-TRE:ChR2-EYFP [(H), (J), (L), and (M)] or AAV9-TRE:EYFP [(I), (O), and (P)]. (**N**) Heat map representing nose position of test mice. (H), n = 10 mice; (I), n = 6 mice; (J), n = 10 mice, (L), n = 10 mice; (M), n = 14 mice; (O), n = 7 mice; (P), n = 7 mice; significance for multiple comparisons: paired t test [(H) to (I)] and ANOVA, post-hoc, Scheffe [(L), M), (O), and (P)], $^{*}P < 0.05$; $^{**}P < 0.01$; n.s., not significant. Data presented as mean ± SEM.

monitored by a social discrimination test. Thus, the vCA1 cells activated by the exposure to a familiar mouse satisfy the criteria to be met by engram cells for a specific memory (*25*). It is interesting that this recall of the social memory by light can occur even after the mice have fallen into an amnesic state. This indicates that the specific social memory information is retained in the specific vCA1 cell population during at least 1 day after encoding but that natural recall cues are not strong enough to reactivate these cells for memory recall; in contrast, the 20-Hz blue light is stronger and reactivates the engram cells above the threshold necessary for recall. This interpretation of light-mediated recall of the social memory is supported by the inception experiment; the social memory is retained in the amnesic mice, and the light-reactivated engram serves as a CS and becomes associated with a high-valence US (footshocks or cocaine) to evoke avoidance or preference behavior.

The present study helps to resolve the controversy (*7*–*9*) regarding the necessity of mouse hippocampus for social memory and corroborates previous observations made in primates (*4*–*6*). In macaques, a large population of neurons in the anterior hippocampus responded to socially relevant cues such as faces and voices of individuals (*6*). In human medial temporal lobe, including the anterior hippocampus, there are cells that respond more to famous or personally relevant people than to unfamiliar people (*4*, *5*). The overall results suggest evolutionary conservation of the role of the hippocampal areas as the sites of social memory.

Recent studies have shown that dCA2 is critical for sociocognitive memory processing (*10*, *11*, *26*). dCA2 neurons have longitudinal rostro-caudal projections to vCA1 (fig. S18) (*27*, *28*) and connect with the deep layer of CA1 more strongly than with the superficial layer (*28*). It is thus possible that the dCA2-vCA1d-NAc circuit composes the engram cell ensemble pathway for social memory (*25*). However, it is also possible that the role of dCA2 in social memory is to convey to vCA1d appropriately processed and socially relevant cues, rather than holding memory information per se.

Compared to other forms of episodic memory, social memory lasts no more than a few hours (Fig. 1C) under laboratory conditions (*29*, *30*), although it can be prolonged to a week by vasopressin release, or to 24 hours by group housing (*12*, *29*, *31*). We have demonstrated by optogenetics that the engram cells for social memory formed in a laboratory environment can be retained in vCA1 for at least 2 days. Thus, the relatively short duration of social memory is apparently due to inefficient retrieval rather than failed retention of the memory. It would be interesting to test the hypothesis that increased vasopressin and/or group housing prolongs social memory duration by promoting the retrieval process.

Overall, our study establishes vCA1 and its NAc projections as a site of social memory and provides insights and clues to the neuronal mechanisms underlying this important form of memory (fig. S19).

REFERENCES AND NOTES

1. L. A. McGraw, L. J. Young, *Trends Neurosci.* **33**, 103–109 (2010).
2. T. Okuyama *et al.*, *Science* **343**, 91–94 (2014).
3. C. N. Smith *et al.*, *Proc. Natl. Acad. Sci. U.S.A.* **111**, 9935–9940 (2014).
4. R. Q. Quiroga, L. Reddy, G. Kreiman, C. Koch, I. Fried, *Nature* **435**, 1102–1107 (2005).
5. I. V. Viskontas, R. Q. Quiroga, I. Fried, *Proc. Natl. Acad. Sci. U.S.A.* **106**, 21329–21334 (2009).
6. J. Sliwa, A. Planté, J. R. Duhamel, S. Wirth, *Cereb. Cortex* **26**, 950–966 (2016).
7. M. von Heimendahl, R. P. Rao, M. Brecht, *J. Neurosci.* **32**, 2129–2141 (2012).
8. A. S. Squires, R. Peddle, S. J. Milway, C. W. Harley, *Neurobiol. Learn. Mem.* **85**, 95–101 (2006).
9. D. M. Bannerman, M. Lemaire, S. Beggs, J. N. Rawlins, S. D. Iversen, *Exp. Brain Res.* **138**, 100–109 (2001).
10. F. L. Hitti, S. A. Siegelbaum, *Nature* **508**, 88–92 (2014).
11. E. L. Stevenson, H. K. Caldwell, *Eur. J. Neurosci.* **40**, 3294–3301 (2014).
12. J. H. Kogan, P. W. Frankland, A. J. Silva, *Hippocampus* **10**, 47–56 (2000).
13. P. Andersen, T. V. Bliss, K. K. Skrede, *Exp. Brain Res.* **13**, 222–238 (1971).
14. B. A. Strange, M. P. Witter, E. S. Lein, E. I. Moser, *Nat. Rev. Neurosci.* **15**, 655–669 (2014).
15. M. S. Fanselow, H. W. Dong, *Neuron* **65**, 7–19 (2010).
16. J. Camats Perna, M. Engelmann, in *Current Opinion in Behavioral Neurosciences*, M. Geyer, B. Ellenbrook, C. Marsden, Eds. (Springer, 2015), pp. 1–21.
17. X. Liu *et al.*, *Nature* **484**, 381–385 (2012).
18. L. G. Reijmers, B. L. Perkins, N. Matsuo, M. Mayford, *Science* **317**, 1230–1233 (2007).
19. T. Kitamura *et al.*, *Science* **343**, 896–901 (2014).
20. Y. Ziv *et al.*, *Nat. Neurosci.* **16**, 264–266 (2013).
21. T. W. Chen *et al.*, *Nature* **499**, 295–300 (2013).
22. S. Ramirez *et al.*, *Science* **341**, 387–391 (2013).
23. F. V. Subach *et al.*, *Nat. Chem. Biol.* **5**, 118–126 (2009).
24. T. J. Ryan, D. S. Roy, M. Pignatelli, A. Arons, S. Tonegawa, *Science* **348**, 1007–1013 (2015).
25. S. Tonegawa, X. Liu, S. Ramirez, R. Redondo, *Neuron* **87**, 918–931 (2015).
26. D. A. Caruana, G. M. Alexander, S. M. Dudek, *Learn. Mem.* **19**, 391–400 (2012).
27. N. Tamamaki, K. Abe, Y. Nojyo, *Brain Res.* **452**, 255–272 (1988).
28. K. Kohara *et al.*, *Nat. Neurosci.* **17**, 269–279 (2014).
29. R. M. Bluthé, G. Gheusi, R. Dantzer, *Psychoneuroendocrinology* **18**, 323–335 (1993).
30. D. H. Thor, W. R. Holloway, *J. Comp. Physiol. Psychol.* **96**, 1000–1006 (1982).
31. A. S. Smith, S. K. Williams Avram, A. Cymerblit-Sabba, J. Song, W. S. Young, *Mol. Psychiatry* **21**, 1137–1144 (2016).

ACKNOWLEDGMENTS

We thank C. Sun, X. Liu, S. LeBlanc, J. Derwin, W. Yu, F. Bushard, S. Huang, G. Das, T. O'Connor, J. Young, and L. Brenner for their help. Supported by the RIKEN Brain Science Institute, Howard Hughes Medical Institute, the JPB Foundation (to S.T.), and Japan Society for the Promotion of Science Grant-in-Aid (to T.O.). All data and computer codes necessary to understand and assess the conclusions of this research are available in the supplementary materials. AAV9-hSyn:DIO-eArchT3.0-EYFP, AAV9-TRE:FT-Slow, AAV9-TRE:ChR2-EYFP, and AAV9-TRE:EYFP were developed at MIT by the group of S.T.; virus plasmids are available through a material transfer agreement. The Trpc4-Cre transgenic mouse line was developed at RIKEN BSI by the group of S.I. and is available through a material transfer agreement.

SUPPLEMENTARY MATERIALS

www.sciencemag.org/content/353/6307/1536/suppl/DC1
Materials and Methods
Figs. S1 to S19
References (*32*–*35*)

16 March 2016; accepted 29 July 2016
10.1126/science.aaf7003

VIROLOGY

MAVS-dependent host species range and pathogenicity of human hepatitis A virus

Asuka Hirai-Yuki,[1,2] Lucinda Hensley,[1,2] David R. McGivern,[1,3] Olga González-López,[1,2] Anshuman Das,[1,2] Hui Feng,[1,2] Lu Sun,[1,2] Justin E. Wilson,[1,2,4] Fengyu Hu,[1,2] Zongdi Feng,[1,2]* William Lovell,[1] Ichiro Misumi,[1,2,4] Jenny P.-Y. Ting,[1,2,4] Stephanie Montgomery,[1,5] John Cullen,[6] Jason K. Whitmire,[1,2,4] Stanley M. Lemon[1,2,3]†

Hepatotropic viruses are important causes of human disease, but the intrahepatic immune response to hepatitis viruses is poorly understood because of a lack of tractable small-animal models. We describe a murine model of hepatitis A virus (HAV) infection that recapitulates critical features of type A hepatitis in humans. We demonstrate that the capacity of HAV to evade MAVS-mediated type I interferon responses defines its host species range. HAV-induced liver injury was associated with interferon-independent intrinsic hepatocellular apoptosis and hepatic inflammation that unexpectedly resulted from MAVS and IRF3/7 signaling. This murine model thus reveals a previously undefined link between innate immune responses to virus infection and acute liver injury, providing a new paradigm for viral pathogenesis in the liver.

Although viral hepatitis is an important cause of human morbidity worldwide, there are no small-animal models that accurately recapitulate liver disease caused by any of the five responsible viruses (*1*, *2*). Previous studies have relied heavily on nonhuman primates, especially chimpanzees (*3*, *4*), to investigate pathogenesis and immune responses to hepatitis viruses. This has handicapped efforts to understand host responses within the unique immunologic environment of the liver (*5*, *6*). Recent NIH policies effectively eliminate the use of chimpanzees